DØ Note 5426-CONF

Search for Light Higgs Boson in $\gamma\gamma + X$ Final State with the DØ Detector at $\sqrt{s} = 1.96$ TeV

The DØ Collaboration
URL http://www-d0.fnal.gov
(Dated: August 9, 2007)

We report the results of a search for a narrow resonance decaying into two photons in 1.1 fb^{-1} of data collected by the DØ experiment at the Tevatron during the period 2002-2006. We find no evidence of such a resonance and set the lower limit on the mass of fermiophobic Higgs Boson of $m_h > 92$ GeV @95% CL. This exclusion limit surpasses Tevatron Run I and Run II results.

Preliminary Results for Summer 2007 Conferences

I. INTRODUCTION

The Standard Model (SM) describes our world at current experimentally accessible energies. However, the exact mechanism for the EWSB remains a mystery. The spontaneous symmetry breaking mechanism is accomplished by a single doublet of complex scalar fields. But does Nature follow this minimalistic version or does it require a multi-Higgs sector or something completely different?

In a more general framework where the parameter content of the theory is richer, we may expect deviations from the SM predictions in the form of significant changes in the Higgs boson discovery signatures. One such example is the so-called "fermiophobic" Higgs boson, which has suppressed couplings to all fermions. It may arise in a variety of models (e.g. [1]). A variation of this theme is the Higgs boson in certain top-color models, which may couple only to heavy quarks [2]. Some even more exotic possibilities have been suggested in the context of theories with large extra dimensions [3]. Finally, in the Minimal Supersymmetric Standard Model (MSSM), the width into $b\bar{b}$ pairs can be suppressed due to 1-loop supersymmetry (SUSY) corrections, thus enhancing the branching ratios of a light Higgs boson into more exotic signatures [4, 5]. In all these cases, for masses $m_h < 100$ GeV the Higgs boson dominantly decays to photon pairs [6]. Decays are mediated through a W or a heavy quark loop.

Experimental searches for fermiophobic higgs (h_f) at LEP and the Tevatron have yielded negative results. Mass limits have been set in a benchmark model that assumes that coupling $h_f VV$ ($V \equiv W^{\pm}, Z$) has the same strength as in the Standard Model and that all fermion Branching Ratios (BR) are exactly zero. Combination of results obtained by the LEP collaborations OPAL [7], DELPHI [8], ALEPH [9], and L3 [10] yielded the lower bound $m_h > 108.3$ GeV at 95% CL. This result was obtained utilizing the process $e^+e^- \to h_f Z,\ h_f \to \gamma\gamma$. In Run 1 of the Tevatron, the lower limits on m_{h_f} from the DØ and CDF collaborations are respectively 78.5 GeV [11] and 82 GeV [13] at 95% C.L., using the processes $qq' \to V^* \to h_f V,\ h_f \to \gamma\gamma$, with the dominant contribution coming from $V = W^{\pm}$. A preliminary search in the inclusive $2\gamma + X$ channel has been performed with 190 pb^{-1} of Run 2a data [16].

In this study we perform a search for the inclusive production of di-photon final states through the mechanisms:

$$p\bar{p} \to VV \to h_f \to \gamma\gamma + X,$$
$$p\bar{p} \to h_f W^{\pm}(Z) \to \gamma\gamma + X.$$

II. SIGNAL SIMULATION

For the generation of the signal process we used leading order generation from the PYTHIA [17] event generator. We use vector boson fusion $VV \to h$ and $q_i\bar{q}_j \to W^{\pm}/Z + h$ associated Higgs production processes with the Higgs restricted to the two photon decay mode but all decay modes of W and Z are included. CTEQ6L1 [20] parton distribution functions are used. The events are passed through the full DØ detector simulation program. The theoretical NLO cross sections obtained with HIGLU program are summarized in Table I [12].

TABLE I: Summary of NLO (HIGLU) cross sections (pb) of fermiophobic Higgs boson for different Higgs masses for various production mechanisms (vector boson fusion and associated production.) and branching ratio for decay into two photons.

mass, GeV	W/Z_{fusion}, pb	$W_{\text{associated}}$, pb	$Z_{\text{associated}}$, pb	$\sigma_{fusion}/\sigma_{\text{associated}}$	σ_{total}, pb	BR($h \to \gamma\gamma$)
70	0.18	0.88	0.47	0.13	1.53	0.81
80	0.15	0.60	0.32	0.16	1.07	0.7
90	0.13	0.42	0.23	0.20	0.78	0.4
100	0.11	0.30	0.17	0.24	0.58	0.18
110	0.09	0.22	0.12	0.27	0.43	0.06
120	0.08	0.16	0.093	0.32	0.33	0.028
130	0.06	0.12	0.071	0.36	0.25	0.02
140	0.06	0.09	0.055	0.41	0.21	0.006
150	0.05	0.07	0.041	0.45	0.16	0.002

III. DATA SAMPLE AND EVENT SELECTION

A. Electrons/Photons/Jets

Photons and electrons are identified in two steps (for a more detailed description of the electron definition see e.g. [18]): the selection of electromagnetic (EM) clusters, and then the subsequent separation into those caused by photons and electrons. EM clusters are selected from calorimeter clusters by requiring that (i): at least 97% of the energy be deposited in the EM section of the calorimeter, (ii): the calorimeter isolation[26] to be less than 0.07, (iii): the transverse shower profile to be consistent with those expected for an EM shower, and (iv) the scalar p_T sum for all tracks originating from the primary vertex in an annulus of $0.05 < R < 0.4$ around the cluster be less than 2 GeV. The cluster is then defined as an electron if there is a reconstructed track (or electron-like pattern of hits in the tracker) associated with it and a photon otherwise. In this analysis we select EM jets (jets with a leading π^0 or η) defined as EM clusters that pass all cuts that are required for photon candidates except failing the track isolation requirement. For convenience we will refer to them as "j" or "jet".

B. Vertex and EM Shower Pointing

Identification of the primary vertex in the event is very important, as it affects the calculation of the p_T of a photon candidate and its track isolation. We select vertex to be withing a coverage of DØ tracker. We also apply a cut on the relative position of the primary vertex and an extrapolated position of the vertex from the central preshower detector (CPS) and the EM calorimeter. The DØ CPS is situated between the solenoid and the EM section of the calorimeter and has enough material in front of it so that the probability for a photon to start a shower before reaching the CPS is high. We fit positions of the EM shower in the four layers of the EM calorimeter and in the CPS to a straight line and extrapolate it to the beam line.

C. Data Selection

In this analysis we use data collected during the period 2002-2007. We select events that fired single EM triggers. They become fully efficient for EM showers with p_T greater than 30 GeV. A Higgs Boson of mass >70 GeV has two energetic photons per event. Fig. 1 illustrates the p_T distributions of the leading and the next-to-leading photons for two Higgs boson masses $m_h = 90$ GeV and $m_h = 150$ GeV. The efficiency for the signal events to satisfy the trigger requirements is $(98 \pm 1)\%$. The total integrated luminosity of the sample is 1100 ± 70 pb^{-1} [19].

We select events that have at least two photons in the central calorimeter ($|\eta| < 1.1$) with a cut on their transverse momenta: ${p_T}^{1,2} > 25$ GeV. Events are required to have the primary vertex with $|z_{vtx}| < 60$ cm from the geometrical center of the detector. Also, at least one of the photons is required to have an associated CPS cluster and point to within 12 cm from the z position from the primary vertex.

IV. DI-PHOTON DATA SAMPLE

The Higgs is expected to be produced with higher transverse energy compared to its backgrounds. We define two study regions – control ($q_T^{\gamma\gamma} < 35$ GeV) and signal ($q_T^{\gamma\gamma} > 35$ GeV), where $q_T^{\gamma\gamma}$ is the transverse momentum of the two photon system. After all selection criteria we are left with 1786 (226) di-photon events in the control (signal) region for invariant masses above 65 GeV.

V. BACKGROUND ESTIMATION

There are several sources of background to the Higgs candidates:

- $\gamma\gamma$ – irreducible background with two real photons coming from the Direct Di-Photon Production (DDP) process.
- γ+jet – instrumental background from $\gamma + g$ or $\gamma + q$ processes where a quark or a gluon fragmented into an energetic π^0 or η and is reconstructed as a photon.
- jet+jet – a multijet background where both photons are faked by jets.
- ee – a background with two real electrons coming from the decay of a Z boson and the electrons fake photons if there is no associated track.

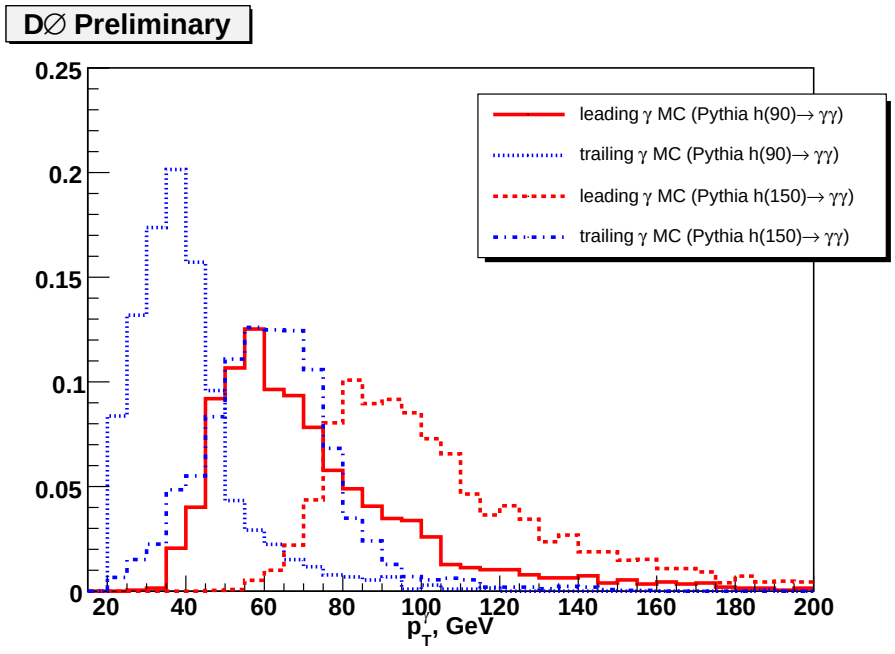

FIG. 1: Normalized distributions of $p_T{}^{\gamma}$ of the leading and the next-to-leading photon for $m_h = 90$ GeV and $m_h = 150$ GeV.

- e+jet(γ)– a background with one real electron coming from the decays of $W^{\pm}$ bosons produced in the association with a real photon or a photon faked by a jet.

The contribution of the events with one or two real electrons has been estimated to be negligible by applying the $e \to \gamma$ to Z+DY and W+X event yields.

We use the MC simulation to predict the γγ background. We estimate relative contributions of the γ+jet and jet+jet backgrounds using the difference in the energy weighted width of the energy deposition in CPS. We will refer to this variable as σ_E^{cps}. One expects a narrow width for photons, and a wider response for jets. This can be seen from the upper-left plot in Fig. 2.

We start with constructing templates for real and fake photons. A template is defined as a distribution of σ_E^{cps} normalized to one. For the real photons' template (G(x$\equiv \sigma_E^{cps}$)) we used $h \to \gamma\gamma$ MC (studies of $Z \to ee$ and $Z \to ll+\gamma$ showed that σ_E^{cps} is reasonably well described by the MC). For the fakes' template (J(x)) we use EM clusters that pass all photon ID cuts except for the track isolation which is reversed. Fig. 2 shows the σ_E^{cps} distribution in the γγ sample before the $q_T^{\gamma\gamma}$ cut, fit by the two templates. To account for the slight disagreement between the data and the fit we vary the fit range and use the spread of the fitted fractions as a systematic error.

To determine the relative fractions of the γγ, γj, and jj components in the γγ data sample we made a two-dimensional distribution of σ_E^{cps} of both photons in the γγ sample (Fig. 3). For each event we randomly decide whether the leading photon will be plotted along the x- or the y-axis. Further we construct three templates that correspond to the 2D σ_E^{cps} profiles in the three components – γγ, γj, and jj:

$$\begin{aligned} GG(x,y) &= G(x)\cdot G(y), \\ GJ(x,y) &= 0.5\cdot(G(x)\cdot J(y)+J(x)\cdot G(y)), \\ JJ(x,y) &= J(x)\cdot J(y). \end{aligned} \tag{1}$$

Further, with these 2D templates we construct a fitting function to determine the individual components in data:

$$F(x,y) = c_0\cdot(GG(x,y)+c_1\cdot JJ(x,y)+c_2\cdot GJ(x,y)), \tag{2}$$

here, parameters are chosen in such a way that c_0 is responsible for the overall normalization and c_1 and c_2 determine the contributions of multijet and γj events relative to γγ.

The results of the fits of the $\gamma\gamma$ distribution (Fig. 3) for the control and the signal regions in different fitting ranges are shown in Table II and Table III. The next step is to use the resulting fractions to predict the expected mass distribution in the $\gamma\gamma$ data sample. Uncertainties in the determination of different components are propagated into the uncertainty on the estimated background by adding them in quadrature with the total uncertainty on the expected number of events in the mass window.

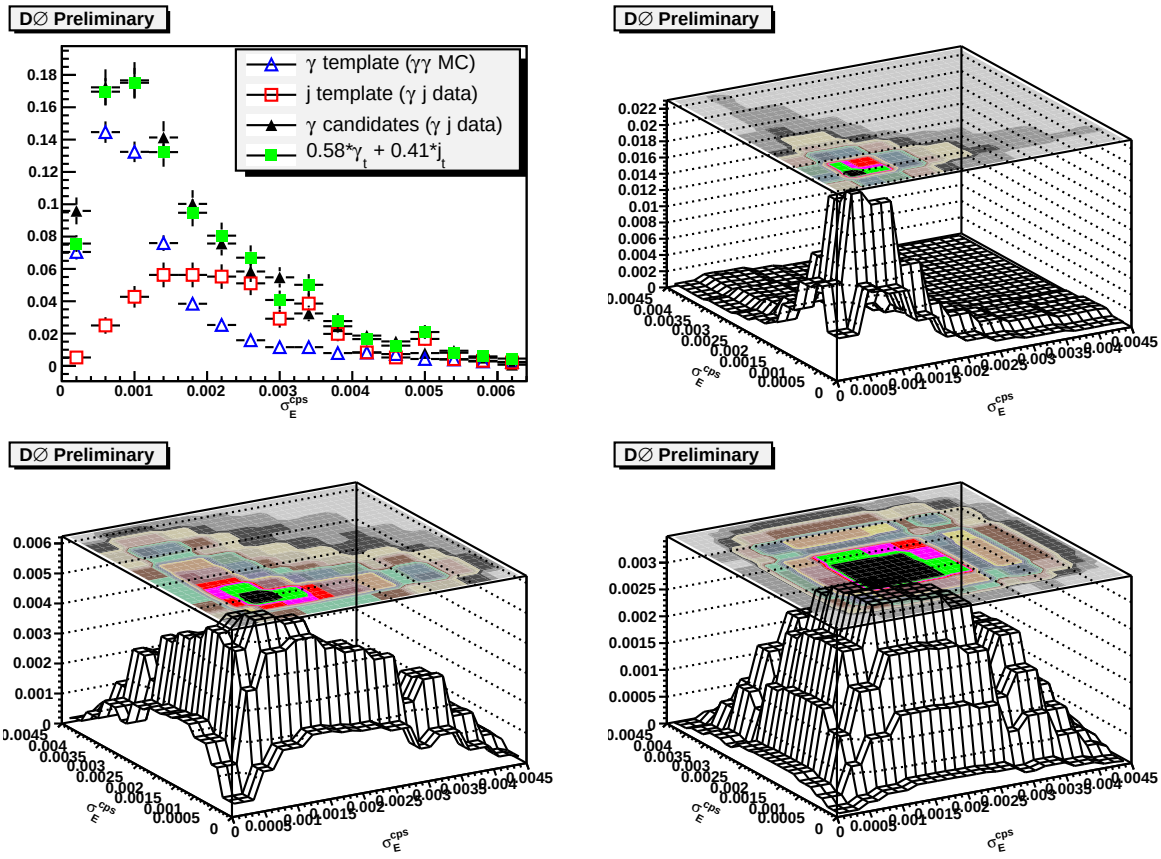

FIG. 2: CPS templates used for the fitting of the di-photon data (Fig. 3). Top Left – normalized distributions of σ_E^{cps} for photons in MC (blue), jets in data (red), and photon candidates in data sample (black). Top right – $\gamma\gamma$ template. Bottom right – jet-jet template. Bottom left – γ-jet template.

As was mentioned above, we take the $\gamma\gamma$ mass distribution from the MC, and γj(GJ) and jj(JJ) templates from data. The total background mass spectrum has the form

$$H(m) = k \cdot N_{\gamma\gamma} \cdot (H_{\gamma\gamma}^{mc}(m) + c_1 \cdot H_{jj}(m) + c_2 \cdot H_{\gamma j}(m)) \tag{3}$$

where $H_{\gamma\gamma}^{mc}$, $H_{\gamma j}$ and H_{jj} are mass templates, c_1 and c_2 are taken from the fit (Eq. 2), $N_{\gamma\gamma}$ is the expected number of $\gamma\gamma$ events given the LO cross-section after it has been corrected by the ResBos/Pythia [23] ratio to account for the NLO corrections. The coefficient k is chosen so that the total number of predicted events is equal to the size of the di-photon data sample, and is equal to 0.91 for the signal region and 0.76 for the control region.

Fig. 4 (control region) and Fig. 5(signal region) illustrate mass distributions in data with the overlaid background predictions. Shaded regions correspond to the expected background error bands. Different colors correspond to the different fits to diphoton purity (see Table II). We take the spread of the predicted numbers of events in the various mass bins as the systematic error on the background determination, and proceed to set a limit on Higgs boson production.

Table IV presents the overal signal acceptance for various mass point that has been corrected for the data/mc effects and the trigger effieciency.

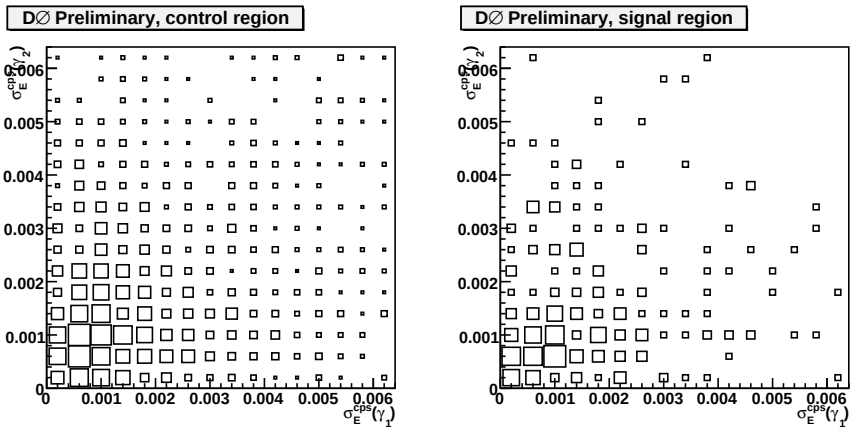

FIG. 3: Distribution of the CPS shower width of one photon vs the other in the control (left) and the signal (right) regions in the data sample.

TABLE II: Control region ($q_T^{\gamma\gamma}$<35 GeV).Values of multijet (c_1) and γj (c_2) fractions defined with respect to the $\gamma\gamma$ component as a result of fits with different fitting limits on CPS width a and b. The first parameter c_0 is the overall normalization constant. For example, with the fitting range of σ_E^{cps} variable between 0.0 and 0.010 (first line of the table), we find that, on average, for every 100 $\gamma\gamma$ events in the diphoton candidate data sample we expect 39 multijet events and 44 γ+jet events.

$\sigma_E^{cps} \in [a,b]$	c_0	c_1	c_2	χ^2/ndf
(0, 0.010)	8.8e+02 $\pm$ 60.2	0.39 $\pm$ 0.05	0.44 $\pm$ 0.118	322/315
(0, 0.007)	8.7e+02 $\pm$ 60.2	0.39 $\pm$ 0.0501	0.44 $\pm$ 0.118	261/254
(0, 0.006)	8.7e+02 $\pm$ 60.6	0.4 $\pm$ 0.0504	0.44 $\pm$ 0.119	208/200
(0, 0.004)	8.6e+02 $\pm$ 62.1	0.37 $\pm$ 0.0549	0.45 $\pm$ 0.127	113/96
(0, 0.0035)	8.7e+02 $\pm$ 62.6	0.39 $\pm$ 0.059	0.44 $\pm$ 0.13	90.5/77
(0.0005, 0.007)	7.3e+02 $\pm$ 72.8	0.45 $\pm$ 0.0653	0.67 $\pm$ 0.189	221/222
(0.0005, 0.004)	7.2e+02 $\pm$ 75.3	0.43 $\pm$ 0.0713	0.68 $\pm$ 0.204	82.1/77

TABLE III: Signal region $q_T^{\gamma\gamma}$>35 GeV).Values of multijet (c_1) and γj (c_2) fractions defined with respect to the $\gamma\gamma$ component as a result of fits with different fitting limits on CPS width a and b. The first parameter c_0 is the overall normalization constant. For example, with the fitting range of σ_E^{cps} variable between 0.0 and 0.010 (first line of the table), we find that, on average, for every 100 $\gamma\gamma$ events in the diphoton candidate data sample we expect 76 multijet events and 13 γ+jet events.

$\sigma_E^{cps} \in [a,b]$	c_0	c_1	c_2	χ^2/ndf
(0, 0.010)	1.1e+02 $\pm$ 24.5	0.76 $\pm$ 0.229	0.13 $\pm$ 0.38	78.9/107
(0, 0.007)	1.1e+02 $\pm$ 24.5	0.76 $\pm$ 0.229	0.13 $\pm$ 0.379	73.1/101
(0, 0.006)	1.1e+02 $\pm$ 24.5	0.77 $\pm$ 0.23	0.12 $\pm$ 0.38	65/92
(0, 0.004)	1.1e+02 $\pm$ 24.5	0.68 $\pm$ 0.235	0.18 $\pm$ 0.404	47/64
(0, 0.0035)	1.1e+02 $\pm$ 24.6	0.64 $\pm$ 0.233	0.16 $\pm$ 0.398	44/57
(0.0005, 0.007)	89 $\pm$ 29.5	1 $\pm$ 0.344	0.23 $\pm$ 0.572	56.3/84
(0.0005, 0.004)	85 $\pm$ 29.6	0.91 $\pm$ 0.348	0.32 $\pm$ 0.631	31.5/49

TABLE IV: Overall MC signal acceptance for various mass points.

mass, GeV	70	80	90	100	110	120	130	140	150
A^{overal}	0.076 $\pm$ 0.006	0.09 $\pm$ 0.007	0.11 $\pm$ 0.009	0.13 $\pm$ 0.01	0.14 $\pm$ 0.01	0.15 $\pm$ 0.01	0.14 $\pm$ 0.01	0.16 $\pm$ 0.01	0.15 $\pm$ 0.01

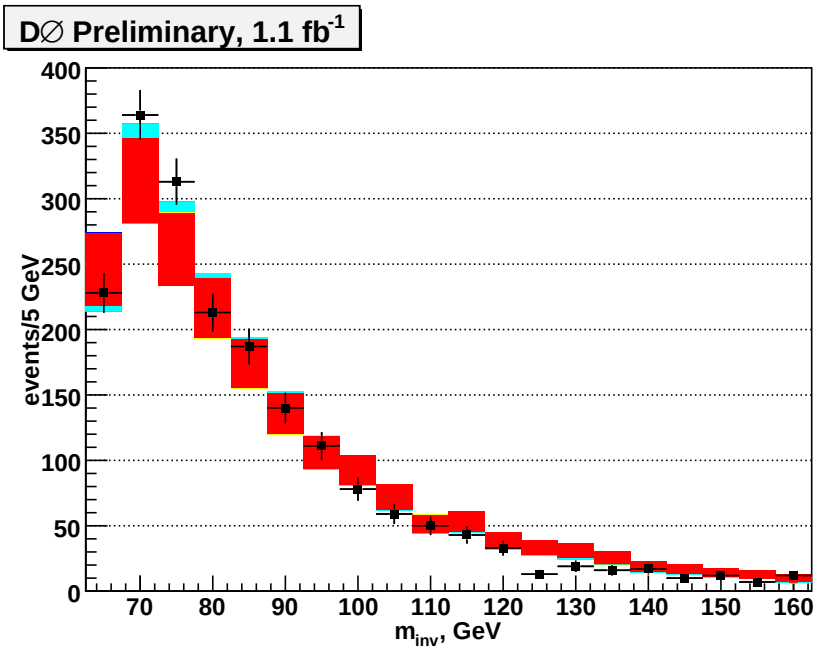

FIG. 4: Diphoton mass distribution in the **control** *region in data (black squares) with the overlaid background predictions. Shaded regions corresponds to the expected background error bands. Different colors correspond to the different diphoton purity fits (see Table II).*

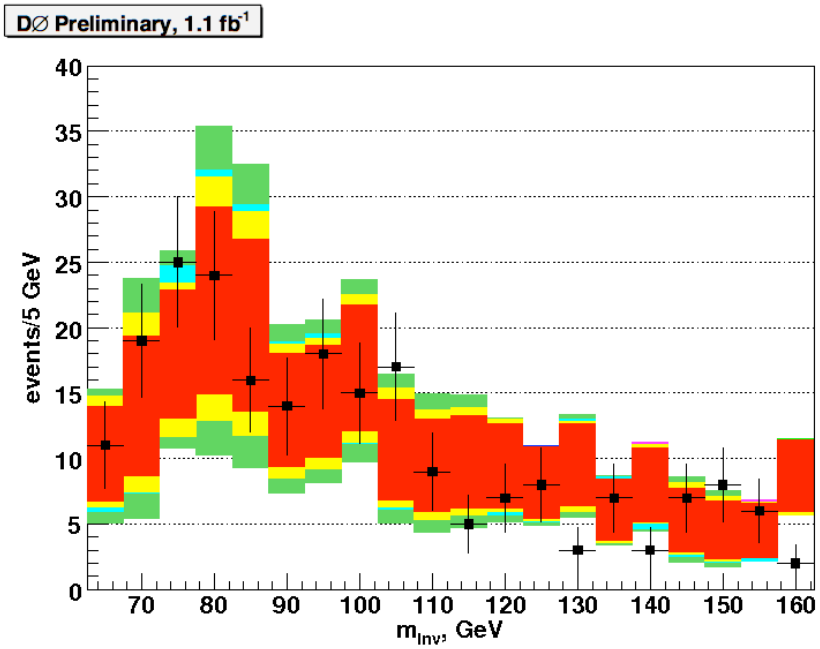

FIG. 5: Diphoton mass distribution in the **signal** *region in data (black squares) with overlaid background predictions. Shaded regions corresponds to the expected background error bands. Different colors correspond to the different diphoton purity fits (see Table III).*

A. Limits

In the absence of an excess of events in the data we proceed with setting an upper limit [24, 25] on the Higgs boson production cross section allowed by this analysis at the 95% confidence level. We use sliding mass window (15 GeV) to count number of observed and background events. Obtained limits are shown in Fig. 6.

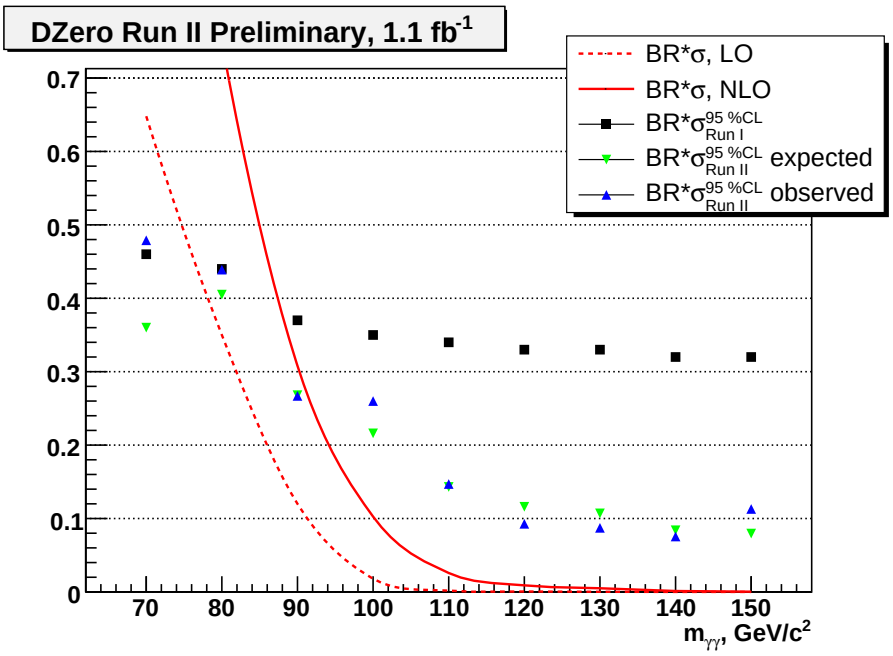

FIG. 6: Comparison of the preliminary results with the Run I DØ results and the theoretical cross section times branching ratio for the benchmark model.

Run I excluded fermiophobic Higgs up to masses of 78.5 (DØ) and 82(CDF) GeV (at 95% CL). Note that those results were obtained using the LO Pythia Higgs production cross section. However, NLO, and NNLO calcualtions raise the theoretical cross sections by a factor of 2-3 thus resulting to higher exclusion values. The present study excludes masses of the fermiophobic Higgs boson up to 92 GeV. This is the most stringent limit to date at hadron colliders.

[1] H. E. Haber, G. L. Kane, and T. Sterling, Nucl. Phys. **B161**, 493 (1979); J. F. Gunion, R. Vega, and J. Wudka, Phys. Rev. D **42**, 1673 (1990); J. L. Basdevant, E. L. Berger, D. Dicus, C. Kao, and S. Willenbrock, Phys. Lett. B **313**, 40(1993); V. Barger, N. G. Deshpande, J. L. Hewett, and T. G. Rizzo, separate Higgs, Report No. OITS-499, hep-ph/9211234; P. Bamert and Z. Kunszt, Phys. Lett. B **306**, 335 (1993); A. G. Akeroyd, 368, 89 (1996) ; M. C. Gonzalez-Garcia, S. M. Lietti, and S. F. Novaes, Phys. Rev. D **57**, 7045 (1998); A. Barroso, L. Brucher, and R. Santos, Phys. Rev. D **60**, 035005 (1999); L. Brucher and R. Santos, Eur. Phys. J. C 12, **87** (2000).

[2] B. Dobrescu, Phys. Rev. D (to be published), Report No. FERMILAB-PUB-99/234-T, hep-ph/9908391; B. Dobrescu, G.Landsberg, and K. Matchev, FERMILAB-PUB-99/324-T.

[3] L. Hall and C. Kolda, Phys. Lett. B **459**, 213 (1999); H. Cheng, B. A. Dobrescu, and C. T. Hill, Electroweak symmetry breaking and extra dimensions, Report No. FERMILAB-PUB-99/358-T, hep-ph/9912343.

[4] M. Carena, S. Mrenna, and C. E. Wagner, Phys. Rev. D **60**, 075010 (1999).

[5] S. Mrenna, talk given at PASCOS99, Lake Tahoe, California, 1999.

[6] A. Djouadi, M. Spira, and P. M. Zerwas, Phys. Lett. B **311**, 255 (1993); A. Stange, W. Marciano, and S. Willenbrock, Phys. Rev. D **49**, 1354 (1994); M. A. Diaz and T. J. Weiler, Decays of a fermiophobic Higgs, Report No. VAND-TH-94-1, hep-ph/9401259; K. Melnikov, M. Spira, and O. Yakovlev, Z. Phys. C **64**, 401 (1994) ; S. Moretti and W. J. Stirling, Phys. Lett. B 347, 291 (1995); Y. Liao and X. Li, 396, 225 (1997); M. Steinhauser, "Corrections to the decay of an intermediate-mass Higgs boson into two photons", Report No. MPI-PHT-96-130, hep-ph/9612395; A. Djouadi, "Decays of the Higgs bosons", Report No. PM-97-51, hep-ph/9712334.

[7] G. Abbiendi *et al.* [OPAL Collaboration], Phys. Lett. B **544**, 44 (2002).

[8] P. Abreu *et al.* [DELPHI Collaboration], Phys. Lett. B **507**, 89 (2001); Eur. Phys. J. C **35**, 313, (2004).

[9] A .Heister *et al.* [ALEPH Collaboration], Phys. Lett. B **544**, 16 (2002).

[10] P. Achard *et al.* [L3 Collaboration], Phys. Lett. B **534**, 28 (2002); Phys. Lett. B **568**, 191 (2003).
[11] B. Abbott et al. [DØ Collaboration], Phys. Rev. Lett. **82**, 2244 (1999).
[12] M.Spira, VV2H, V2HV programs, http://people.web.psi.ch/spira/proglist.html
[13] T. Affolder et al. [CDF Collaboration], Phys. Rev. D **64**, 092002 (2001).
[14] V. M. Abazov et al. [D0 Collaboration], arXiv:hep-ex/0508054.
[15] G. Landsberg and K. T. Matchev, Phys. Rev. D **62**, 035004 (2000).
[16] A. Melnitchouk [D0 Collaboration], Int. J. Mod. Phys. A **20**, 3305 (2005).
[17] Sjöestrand, T. *et al.*, PYTHIA 6.3 Physics and Manual, hep-ph/0308153 (2003).
[18] http://www-d0.fnal.gov/Run2Physics/WWW/results/final/TOP/T07D
[19] T. Andeen *et. al.*, FERMILAB-TM-2365-E (2006)
[20] CTEQ6 Parton Distributions, hep-ph/0512167 (2005).
[21] F. Maltoni, Madevent: Automatic Event Generation with MADGRAPH, hep-ph/0208156 (2002).
[22] G. C. Blazey et al., in Proceedings of the Workshop: "QCD and Weak Boson Physics in Run II" edited by U. Baur, R. K. Ellis, and D. Zeppenfeld, 47 (2000). See Section 3.5 for details.
[23] C. Balazs, C.P. Yuan. Phys. Rev. D**56**:5558, 1997. [arXiv:hep-ph/9704258]
[24] http://www-d0.fnal.gov/Run2Physics/limit_calc/limit_calc.html
[25] R.T. Cox, Am. J. Phys. **14**, 1 (1946); H. Jeffreys, "*Theory of Probability*", 3rd edition, Oxford University Press (1961); E.T. Jaynes and L. Bretthorst, "*Probability Theory, the Logic of Science*", Oxford, 2003; A. O'Hagan, "*Kendall's Advanced Theory of Statistics, Volume 2B: Bayesian Inference*", Oxford (1994).
[26] Isolation is defined as $[E_{tot}(0.4) - E_{EM}(0.2)]/E_{EM}(0.2)$, where $E_{tot}(0.4)$ is the total shower energy in a cone of radius $R = \sqrt{(\Delta\eta)^2 + (\Delta\phi)^2} = 0.4$, and $E_{EM}(0.2)$ is the EM energy in a cone $R = 0.2$